Brain Topography (2019) 32:720–740
https://doi.org/10.1007/s10548-018-0619-x

ORIGINAL PAPER

ERP Source Analysis Guided by fMRI During Familiar Face Processing

Maria A. Bobes[1,2] · Agustin Lage-Castellanos[2,4,5] · Ela I. Olivares[3] · Jhoanna Perez Hidalgo-Gato[2] · Jaime Iglesias[3] · Ana Maria Castro-Laguardia[2] · Pedro Valdes-Sosa[1,2]

Received: 19 July 2017 / Accepted: 12 January 2018 / Published online: 20 February 2018

Abstract

Event related potentials (ERPs) provide precise temporal information about cognitive processing, but with poor spatial resolution, while functional magnetic resonance imaging (fMRI) reliably identifies brain areas involved, but with poor temporal resolution. Here we use fMRI to guide source localization of the ERPs at different times for studying the temporal dynamics of the neural system for recognizing familiar faces. fMRI activation areas were defined in a previous experiment applying the same paradigm used for ERPs. The Bayesian model averaging (BMA) method was used to estimate the generators of the ERPs to unfamiliar, visually familiar, and personally-familiar faces constraining the model by fMRI activation results. For this, higher prior probabilities in the solution space were assigned to the fMRI-defined regions, which included face-selective areas and other areas related to "person knowledge" retrieval. Source analysis was carried out in three-time windows: early (150–210 ms), middle (300–380 ms) and late (460–580 ms). The early and middle responses were generated in fMRI-defined areas for all face categories, while these areas do not contribute to the late response. Different areas contributed to the generation of the early and middle ERPs elicited by unfamiliar faces: fusiform (Fus), inferior occipital, superior temporal sulcus and the posterior cingulate (PC) cortices. For familiar faces, the contributing areas were Fus, PC and anterior temporal areas for visually familiar faces, with the addition of the medial orbitofrontal areas and other frontal structures for personally-significant faces. For both unfamiliar and familiar faces, more extended and reliable involvement of contributing areas were obtained for the middle compare with early time window. Our fMRI guide ERP source analysis suggested the recruitment of person-knowledge processing areas as early as 150–210 ms after stimulus onset during recognition of personally-familiar faces. We concluded that fMRI-constrained BMA source analysis provide information regarding the temporal-dynamics in the neural system for cognitive processsing.

Keywords ERPs · BMA · fMRI-constrained source analysis · Familiar faces.

Introduction

Event related potentials (ERPs), have been extensively used to study cognitive processing due to their excellent temporal resolution (millisecond level) that is essential to discover the

Handling Editor: Laura Astolfi.

This is one of several papers published together in Brain Topography on the "Special Issue: Controversies in EEG Source Analysis".

✉ Maria A. Bobes
antonieta@cneuro.edu.cu

✉ Pedro Valdes-Sosa
pedro.valdes@neuroinformatics-collaboratory.org

[1] The Clinical Hospital of Chengdu Brain Science Institute, MOE Key Lab for Neuroinformation, University of Electronic Science and Technology of China, Chengdu, China

[2] Cuban Center for Neuroscience, CNEURO, Ave 25 # 15202, esq. A 158 Cubanacan, CP-11600 apartado 6412–6414, Havana, Cuba

[3] Psychology Faculty, Autonomous University of Madrid, Madrid, Spain

[4] Department of Cognitive Neuroscience, Faculty of Psychology and Neuroscience, Maastricht University, Maastricht, The Netherlands

[5] Maastricht Brain Imaging Center, Maastricht University, Maastricht, The Netherlands

temporal dynamics of brain information processing circuitry. They are hampered however by their low spatial resolution which precludes the extraction of precise anatomical information. On the contrary, functional magnetic resonance imaging (fMRI) provides this detailed anatomical information at the expense of very poor temporal resolution.

Both techniques have been applied to the study of familiar face recognition. Face processing is critical for social interactions. It requires, not only the visual processing of faces, but also access to aspects of person knowledge and emotions, involving the activation of a widespread distributed network of brain areas not well understood yet. It is therefore not surprising that both ERPs and fMRI analyses have been applied to the study of familiar face recognition process—but usually in independent studies, thus yielding information on either spatial or temporal properties in isolation but not both concurrently.

Several ERPs components, occurring at different time latencies, have been related to face processing (see review by Michel et al. 2004). The N170 component seems to be related with structural face processing (Bentin and Deouell 2000) and are not modulated by familiarity (Henson et al. 2003; Eimer 2000a, b, 2011). Late components, mostly around 250–300 ms (and in some cases even later), are modulated by familiarity (Bentin and Deouell 2000; Eimer 2000b; Henson et al. 2003). It is to be noted that the N250 component is associated with individual face recognition (Schweinberger et al. 2002; Kaufmann et al. 2009; see Schweinberger 2011 for review). Our group (Bobes et al. 2007) have used ERPs to uncover a sequence of temporally distinct stages related to aspects of familiar faces processing, i.e. emotion derived from identity at around 300 ms, and visual familiarity at around 500 ms. In summary, ERPs results (including our own) suggest that the processing of information of the familiarity of faces takes place after structural processing has been completed. Nevertheless, due the poor spatial information of ERPs it is challenging to make precise inference about the neural circuits underlying these two types of processing.

On the other hand, fMRI studies have pinpointed the anatomy of the neural circuitry underlying familiar face recognition. The locations involved are separated into two clusters: the core and the extended neural system (Gobbini and Haxby 2007; Haxby et al. 2000). The core system mediates the primary visual analysis of faces and comprises structures in the ventral occipito-temporal cortex, the occipital face area (OFA), the fusiform face area (FFA), and the posterior superior temporal sulcus (pSTS). The extended system, involved in processing information related to familiarity, includes the medial orbitofrontal cortex, insula, anterior cingulate, posterior cingulate cortex, hippocampus and the amygdala (Gorno-Tempini and Price 2001; Leveroni et al. 2000; Elfgren et al. 2006; Henson et al. 2003; Rotshtein et al. 2005; Pourtois et al. 2005a, b; Gobbini et al. 2004; Brambati et al. 2010). The extended system is thought to receive and elaborate input from the core face processing system in ventral occipito-temporal cortex. However, fMRI data do not provide precise spatio-temporal dynamics about the sequence of activation of different nodes.

It would be ideal to combine the estimation of spatial localization with timing of dynamics. One way to extract more anatomical information from the scalp ERPdistribution (denoted by v) is by estimating the sources (Primary Current Densities or PCDs, denoted by j) in the brain that generate the voltage recorded at the scalp by solving the EEG Inverse Problem (IP). The indeterminacy of source localization may be overcome by incorporating prior information (or constraints) regarding EEG generators in order to increase the possibility of obtaining a unique and physiologically valid solution. These constraints are usually expressed as prior probabilities on the sources.

Previous approaches in this direction constraint the possible EEG PCDs to be localized in the gray matter and impose different spartsity models on the spatial distribution of activations. This type of source localization has been used to study the generators of the face related components. In particular, the sources of N170 face sensitive components have been estimated using dipolar (Joyce and Rossion 2005; Kaufmann et al. 2009; Schweinberger et al. 2002; Linkenkaer-Hansen et al. 1998; Jemel et al. 2009; Deffke et al. 2007) and distributed source localizers (Itier and Taylor 2004; Herrmann et al. 2005; Corrigan et al. 2009; Pizzagalli et al. 2002; Latinus and Taylor 2006; Caldara et al. 2003). These studies suggest the FFA and STS as the N170 generators. There has been less work on source analysis of face familiarity ERPs (Schweinberger et al. 2002; Jemel et al. 1999; Rossion et al. 1999; Mnatsakanian and Tarkka 2004) though they point to the fusiform area as the main contributor to the N250 generation (see also Kaufmann et al. 2009). This line of work ignores information about fMRI activation maps.

This has been partially remedied correlating aspects of the N170 with fMRI responses during studies of unfamiliar face with both modalities recorded in the same subjects and with the same paradigm (Horovitz et al. 2004; Pizzagalli et al. 2002; Eryilmaz et al. 2007; Iidaka et al. 2006; Corrigan et al. 2009). These demonstrated reliable relationships between N170 and fMRI functional activation in FFA.

Such comparisons fall short of formally incorporating fMRI activation (with its higher anatomical resolution) as a constraint into the source localization formalism. One interesting approach, known as fMRI-constrained analysis, does uses fMRI as a "hard constraint", limiting source analysis to those locations with significant activations in the fMRI analysis (Dale and Sereno 1993). Thus, for a given segmentation of the brain (say the AAL segemention used in this

paper), an "anatomical model" is the set of regions over which we will allow the search for inverse solutions—in this case those limited to having the fMRI activation of interest.

This "hard threshold" method of selecting the IP anatomical model has been applied to studies of facial expression processing to estimate sources of N170 (and later components) (Pizzagalli et al. 2002; Trautmann-Lengsfeld et al. 2013), gives results congruent with the previously mentioned fMRI studies. Unfortunately, this 'hard-thresholding' approach suffers from an important drawback. By selecting the anatomical model (M) that comprises those areas with fMRI activations, it rule out completely any other source that might be present but invisible to fMRI. This is always an anatomical model larger than that defined by the "hard threshold". Thus we actually have to deal with a number N_m of alterantive possible anatomical models M_m, indexed by $m = 1, \cdots, N_m$—a problem we shall term "anatomical model uncertainty".

A technique that addresses anatomical model uncertainty is Bayesian Model Averaging (BMA), developed by Trujillo-Barreto et al. (2004, see "Material and Methods" sections for a detailed explanation). In BMA each model is defined by the set of assumptions of the inverse method used, as well as by the functional dependence between the data and the Primary Current Density (PCD) inside the brain. This model eliminate depence of the solution on the anatomical model by averaging all estimated PCD weighted by their evidences.

Thus a unique PCD distribution is found that is not conditioned on any particular anatomical model, solving the uncertainty problem. Furthermore, by assigning prior probabilities derived from fMRI activations to anatomical region, a "soft thresholding" based on fMRI activation is implemented, in which regions invisible to BOLD but supported strongly by the ERP information may be included in the final solution. This contrasts with the usual approach to the EEG IP which selects the solution as ignores the model evidence. The efficacy of BMA has been extensively tested with synthetic and real data from simple sensory stimulation with known primary sensory sources with a great improvement over model selection methods as described (Trujillo-Barreto et al. 2004). Even less blurred solutions were obtained when the information from fMRI data was taken into account, thereby highlighting the strong potential of this method for conducting fMRI-"soft-thresholded" ERP source analysis (Penny et al. 2006).

Here we use the innovative BMA method to explore the contributions of fMRI predefined regions of interest (ROIs) to the generation of ERP responses. To this end, we use fMRI and ERP data collected from the same subjects using similar paradigms (in non concurrent experimental sessions). ERPs and fMRI data provided complementary information regarding the face processing system. While fMRI data are used to localize specific ROIs involved in face recognition, ERP data are used to characterize the time-course of face information processing. We estimated the generators of the early (150–210 ms), middle (300–380 ms) and late (460–580 ms) time windows responses using the BMA method, favoring the solution to the fMRI predefined ROIs, but not strictly excluding all other possible anatomical locations. We hypothesized that a subset of the areas detected in the fMRI study (Bobes et al. 2013) contributes to the generation of each ERP component (Bobes et al. 2007). By using the fMRI-constrained BMA approach we were able to estimate the latency of activation in each face area (rather than only localize ERP generators) thus providing information about the temporal dynamics of the familiar face processing.

Materials and Methods

In this article, we combined data from a previous ERP study (Bobes et al. 2007), and a previous event related fMRI study (Bobes et al. 2013). We carried out a new source analysis of the ERPs components using the results of the fMRI study for modeling the solution space for source estimation. Both studies were carried out using the same stimulus material and similar paradigms in different experimental sessions one week apart. The same group of participants was recruited for both experiments, except for two participants, who were not able to participate in the fMRI study and had to be replaced. Details about the event related fMRI experiment (participants, paradigm, acquisition parameters and analysis) could be found in the original paper (Bobes et al. 2013).

fMRI group analysis were used for extracting the fMRI-defined ROIs (19 areas). These ROIs were extracted from two different contrast (Fig. 1a): (1) unfamiliar faces > non faces, which reveal the face-selective areas (the core face system) and (2) personally-familiar faces > unfamiliar faces, which reveal those areas involved in further processing of familiar faces information (the extended face system). In order to obtain larger ROIs for both contrasts, functional areas were selected as the anatomical regions presenting functional activation using a relaxed threshold of $p < 0.005$ (uncorrected). The AAL atlas (Tzourio-Mazoyer et al. 2002) was used for the anatomical segmentation.

Here, we reanalyzed the ERP data from (Bobes et al. 2007), to estimate the specific contributions of these 19 face-activated areas to the generation of ERP responses in three time windows: early (150–210), middle (300–380) and late (460–580) (see Fig. 1b).

Participants

Ten healthy adults, 6 males and 4 females, with ages ranging from 23 to 33 years (*mean* = 27) participated in the ERP study as non-paid volunteers. All participants had university

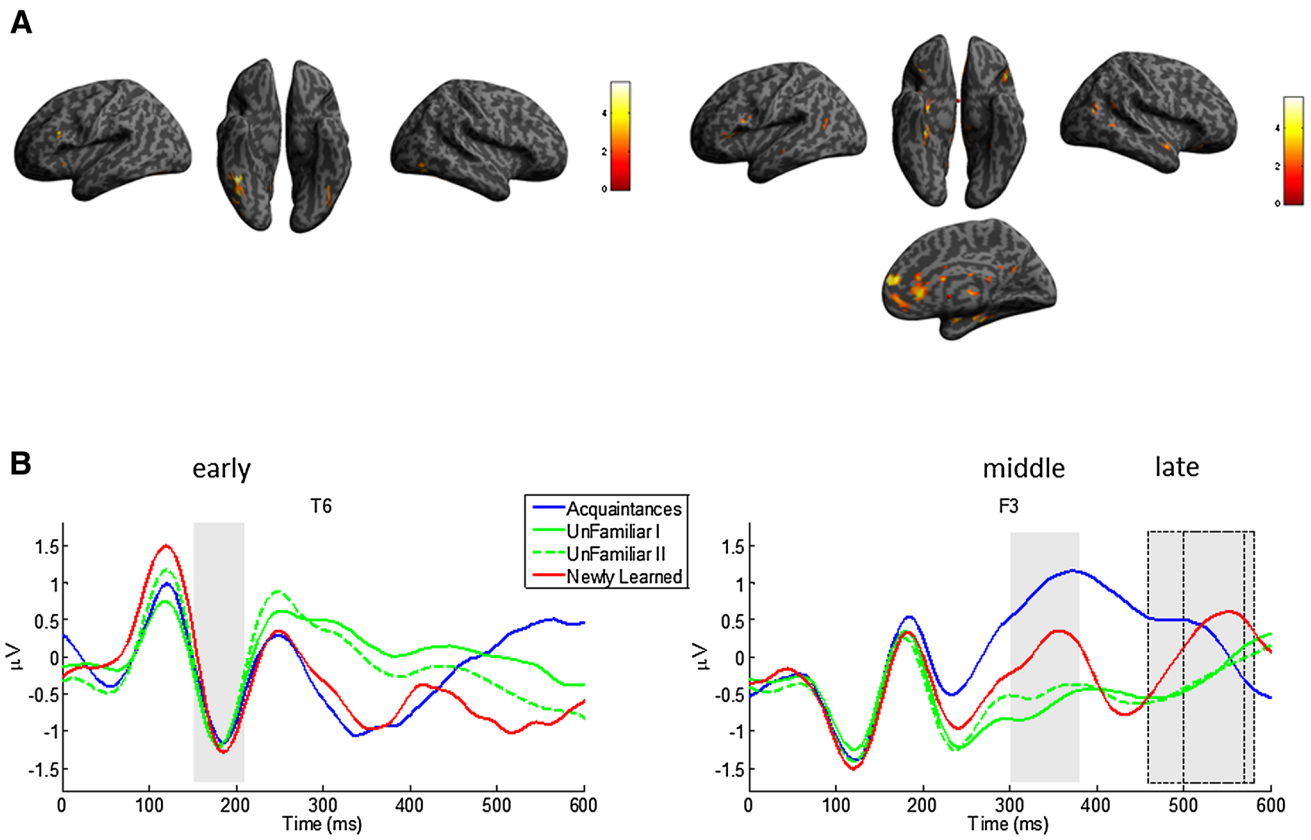

Fig. 1 **a** Activation maps obtained from the fMRI group level analysis in the event related fMRI study (Bobes et al. 2013). In the left panel contrast unfamiliar faces > non faces. In the right panel contrast personally-familiar faces > unfamiliar faces. These activations are shown on an inflated brain, depicting voxels surviving $p < 0.005$ (uncorrected). **b** ERPs recorded at T6 and F3 to faces of acquaintances (in blue), newly-learned faces (in red) and unfamiliar faces (in green). The three time windows used for source analysis are displayed at T6 (early response) and F3 (middle and late responses) electrodes

degrees, all were right-handed (as ascertained by personal report) and all had normal or corrected-to-normal vision. The experimental protocols were approved by the Ethics Committee of the Cuban Neuroscience Center. Participants provided written informed consent to participate in the study, which were documented in signed forms.

Face Stimuli

Stimuli consisted of digitized black and white photographs of faces that could be either familiar or unfamiliar to the participants. Two different sets of familiar faces were obtained, *acquaintance faces*, which were personally familiar faces selected among the family and close friends of each subject (i.e. these faces were different for each participant), and *newly-learned faces*, which were pre-experimentally unfamiliar faces that had been learned in the lab (see Bobes et al. 2007, for a more detailed description). The ERP procedure consisted of two stimulation blocks each, with an oddball paradigm in which one category of familiar faces were randomly mixed with unfamiliar ones. In Block I *acquaintance* and *unknown* faces were combined, with acquaintance faces acting as familiar targets. In Block II, *newly-learned* and *unfamiliar* faces were combined, and the learned faces were the target stimuli. Each block included 15 different familiar and 75 different unfamiliar face identities, and each face image was presented twice, comprising a total of 30 familiar (16.7%) and 150 unfamiliar (83.3%) face trials for each stimuli block. Different unfamiliar faces were used as standards in each block and block order was counterbalanced across subjects. Face stimuli were presented for 1000 ms, with an inter-stimulus interval (ISI) of 1000 ms. Participants were required to discriminate between familiar and unfamiliar faces and respond on the computer keyboard during the ISI (a go/go design).

Data acquisition was carried out with 120 monopolar derivations, homogeneously distributed over the scalp. Two channels for EOG recording were also used. A notch filter with peak at 60 Hz was used and the signals were amplified by a factor of 10,000 and filtered between 0.5 and 30 Hz (3 dB down). All electrodes were referred to linked earlobes

and then re-referenced to an average reference. The inter-electrode impedance was always below 10 kΩ. The onset of the stimuli served to synchronize data collection. The EEG was digitally recorded at a sampling rate of 200 Hz, with 700 ms epochs, and a 300 ms pre-stimulus baseline. EOG correction and artifact rejection were carried out before the ERPs were averaged. Averaged evoked responses were digitally low-pass filtered (5.5 Hz cut-off). ERP amplitudes were corrected by subtracting the average pre-stimulus amplitude value. Additional details of stimulation and recordings can be found in Bobes et al. (2007). In order to equalize the signal to noise ratio for unfamiliar ERP, here we obtained a new average in each subject by randomly selecting 30 trials of this condition.

ERPs resulting from this analysis are displayed in Fig. 1b. These waveforms showed the N170 component, present for all face conditions (mean peak latency 180 ms at T6 electrode), and two different components related to familiarity: one around 350 ms at F3, only present for faces of acquaintances and another around 500 ms at Pz, elicited by newly-learned and acquaintances faces. According to this, we selected three different time windows for sources analysis, which were located around the mean peak latency of each component for all participants and conditions (see shadowed area in Fig. 1b). The early time window was set between 150 and 210 ms (60 ms around N170 component). Since familiarity effect was more extended in time, the middle and late time windows were set between 300 and 380 ms and between 460 and 580 ms, centered around the peak for newly-learned (500–580) and for acquaintances (460–570). These two time windows showed a significant familiarity effect on a permutation tests for the amplitude differences between ERPs for familiar (acquaintances and learned, respectively) and unfamiliar faces. A detailed description of the methods can be found in the previous article (see Bobes et al. 2007).

Source Analysis by Bayesian Model Averaging

ERP Voltage Distributions

Inverse solutions were calculated from the mean amplitude across the three time windows selected (Fig. 1b) for each face condition. For unfamiliar faces two sets of inverse solutions were obtained (each one corresponding to the unfamiliar faces of each block in each subject), which were averaged within subject in order to obtain a set of solutions similar to those obtained for the other face categories. This procedure allow to obtain inverse solutions from ERPs more similar in signal to noise ratio to that present in the two other conditions.

Individual ERPs obtained for each condition in each participant were submitted to source analysis. These individual solutions were later submitted to statistical analysis (see below) which allow the identification of replicable sources across the sample.

Bayesian Model Averaging (BMA)

The principle of BMA is quite simple, and can be understood by noting that all EEG IPs, if we assume a *fixed* anatomical model M_m, can be formulated via Bayes theorem:

$$P\left(j_m \middle| v, \sigma_e^2, \sigma_j^2; M_m\right) = \frac{P\left(v \middle| j_m, \sigma_e^2; M_m\right) P\left(j_m \middle| \sigma_j^2; M_m\right) \left(\sigma_e^2 \middle| M_m\right) \left(\sigma_j^2 \middle|; M_m\right)}{P\left(v \middle| M_m\right)} \quad (1.1)$$

This relation states the a-posteriori probability of the PCD j_m for anatomical model m, defined by the conditional density function $P\left(j \middle| v, \sigma_e^2, \sigma_j^2; M_m\right)$, given the voltage data v and the hyperparameters σ_e^2(sensor noise variance) and σ_j^2 (source variance or strength) is equal to:

- the product of $P\left(v \middle| j_m, \sigma_e^2; M_m\right)$, the likelihood of the data given the PCD, times the prior distributions for the hyperparameters
- divided by the "Evidence" or probability of the data given anatomical model $P\left(v \middle| M_m\right)$.

If there is no doubt about the anatomical model, the best estimate of the PCD ($\hat{j}_m$) is obtained by first estimating the hyperparameters and then maximizing the numerator of (1.1) to obtain what is known as the maximum a posteriori (MAP) estimator of j. This is the standard operating procedure for the EEG IP.

Now consider that we have anatomical model uncertainty: that is we are considering models $m = 1, \ldots, N_m$ models M_m. We now have two choices:

1. Model selection: We pick the $\hat{j}_m$ that has the largest evidence $P\left(v \middle| M_m\right)$.
2. Bayesian model averaging: Eliminate depence of the solution on the anatomical model by averaging all $\hat{j}_m$, weighted by their evidences.

Anatomical Models

The intracerebral PCDs, j is defined over a source space (grid) comprising 17,759 generators. These were placed in R_r $r = 1, \ldots, 20, 19$ corresponding with the face-responding ROIs obtained from the group level analysis of the fMRI data of our previous study, (Bobes et al. 2013) and one including the rest of the brain. The face-responding fMRI-defined

regions were: inferior occipital gyrus (InfOcc), fusiform gyrus (Fus), posterior part of the superior temporal sulcus (pSTS), posterior cingulate cortex (PC), anterior cingulate cortex (AC), middle orbitofrontal (mOF) cortex, inferior frontal cortex pars triangularis (FrInfT), insula (Ins), hippocampus (Hip) and the anterior part of the right temporal middle gyrus (ATempM) (see Fig. 2).

The anatomical model m is defined as a union of any set I of regions:

$$M_m = \bigcup_{I \subset 1,\ldots,20} R_i$$

It to be noted that the number of anatomical models is $Nm = 2^{20}$.

c-Loreta

The basic bulding block for BMA is, in this case, the antomically "constrained LORETA" (cLORETA, see Trujillo-Barreto et al. 2004):

$$\begin{aligned} v &= K_m j_m + e \\ e &\sim N\left(0, \sigma_e^2\right) \\ j &\sim N\left(0, \sigma_j^2 L_m^{-T} L_m^{-1}\right) \\ \sigma_e^2, \sigma_j^2 &\sim IG(\theta) \end{aligned} \tag{1.2}$$

Where $N\left(\mu, \sigma^2\right)$denotes the gaussian distribution defined by the mean and variance. Also v is the voltage distribution of the ERP, and j_m, K_m and $L_m^{-T}$are, respectively, the PCD, lead field and Laplacian operator restricted by the anatomical model m. The hyperparameters are σ_e^2, the sensor noise and σ_j^2 the variance of the sources and are given the usual inverse gamma distribution.

The lead field $K_m$that relates the intracerebral activity to the scalp electric fields was computed. The forward model used in this case consisted of three spheres modeling piecewise homogenous compartments: brain, skull, and scalp. The conductivity values selected in our case were 0.33, 0.022 and 0.013 Ω/m for the brain, scalp, and skull, respectively (Oostendorp et al. 2000; Zhang et al. 2006).

The c-LORETA solution then the MAP estimator:

$$\hat{j}_m = \arg\max_{j_m} P\left(j_m \middle| v, \sigma_e^2, \sigma_j^2; M_m\right) \tag{1.3}$$

This estimator can be reformulated in the more familiar minimization of:

$$\hat{j}_m = \arg\min_{j_m} \frac{1}{\sigma_e^2}\left\|v - K_m j_m\right\|^2 + \frac{1}{\sigma_j^2}\left\|L_m j_m\right\|^2 \tag{1.4}$$

Note that the solution depends on the hyperparameters. Rather than using usual methods such as the generalizaed crossvalidation (GCV) to estimate these parameters, we relied on the iterative procedure developed by MacKay (1992) for this purpose (explained in Trujillo-Barreto et al. 2004).

Model Averaging

The final model of the neural generators associated with the electrophysiological effects was carried out using the

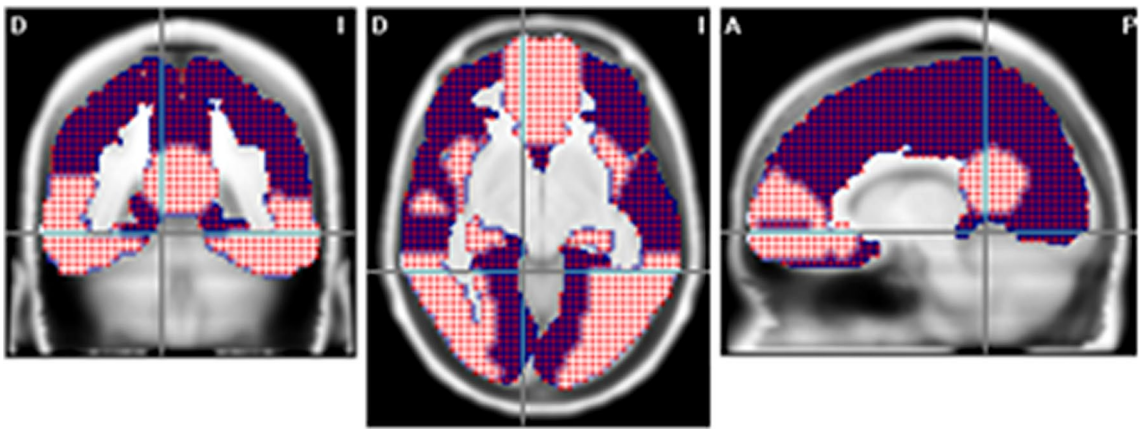

Fig. 2 Source space generators (in red) overlaid on the 20 compartments used for BMA solution estimation. In white the 19 functional face ROIs and in blue the non-specific face areas. Functional face ROIs are left and right inferior occipital gyrus (InfOcc), left and right fusiform gyrus (Fus), right posterior part of the superior temporal sulcus (pSTS), posterior cingulate cortex (PC), anterior cingulate cortex (AC), middle orbitofrontal (mOF) cortex, inferior frontal cortex pars triangularis (FrInfT), insula (Ins), hippocampus (Hip) and the anterior part of the right temporal middle gyrus (ATempM)

Bayesian model averaging (BMA) approach (Penny et al. 2006; Trujillo-Barreto et al. 2004).

The prior probability of each model is expressed in terms of combinations of anatomical compartments defined with independence of the observed data. The final primary current density is obtained as linear combinations of N_m models:

$$\hat{j} = E(j|v) = \sum_{m=0}^{Nm} E\left(j_m|v, M_m\right) p(M_m|v)$$

Where $E(j_m|v, M_m)$is the PCD estimate for modelM_m and $p\left(M_m|v\right)$is the posterior probability of the model M_m given the voltage v which is obtained from the Bayesian expression:

$$p\left(M_m|v\right) = \frac{\alpha_m B_{m0}}{\sum_{l=0}^{Nm} \alpha_l B_{l0}}$$

In this expression, the B_{k0} corresponds to a Bayes factor that measures a ratio of evidences for comparing a model k versus a reference model indexed by 0.

From this description it should be clear that this inverse solution is data-adaptive. In particular for each time window the solution adapts best to the evidence at those latencies.

Note that the reference model $M_0 = \bigcup R_i$ comprise the whole brain. The terms $\alpha_l$are prior odds that define the belief of each anatomical compartment to be involved in the generation of the component. In this case, the prior probability of the fMRI based anatomical compartments was set as $\alpha_l = 1$, while the probability of the rest of the brain was fixed as$\alpha_l = 0.5$. This is the basis of the "soft thresholding" since no area is assigned an $\alpha_l = 0$.

It is easy to see that a "hard thresholding" solution is a particular case of BMA in which only one anaotimical model is considered and prior probabilities are set to zero for many regions.

Group Analysis of Source Reconstruction Maps

The ranks of inverse solution coefficients were computed for each participant. The rank function is defined as the position of each generator in the list that results when the inverse solution coefficients are sorted in descending order. If inverse solution maps are not consistent across participants, a uniform distribution of rank values is expected for each generator across the set of participants. On the contrary, when generators with the largest inverse solution coefficients are concentrated into a particular ROI across subjects, the smallest ranks are expected in this region and a violation of uniformity is obtained.

To evaluate whether the null hypothesis of a uniform distribution of ranks can be rejected, a Kolmogorov–Smirnov (KS) statistics test was used (left tail). The *p-values* of KS statistics were computed with a permutation test with 10,000 repetitions. For each permutation step the ranks of the coefficients of the inverse solution maps were spatially randomized across generators for each participant. This procedure estimates empirically the distribution of KS statistics for the inverse solution coefficients under the null hypothesis of a uniform distribution of ranks. An alpha level of 0.001 was used to extract generators with significant spatial consistency across participants.

The results of the group analysis was summarized at each ROI with the cluster-mass index (Bullmore et al. 1999), which integrates the extent and amplitude of the generators within each ROI. After thresholding the KS statistic map ($p < 0.001$), the resulting inverse solution image is segmented in continuous clusters. At each cluster the sum of KS statistics across all active generators is computed, after subtracting the value of the used statistical threshold. Thus, each ROI is summarized with the cluster mass value within the ROI. It is important to note that the spatial smoothness of the inverse solution maps produces only one cluster at each ROI.

Zmax

For summarizing the results of each cluster the peak of statistical significance of each cluster (p-value min which produces Z-max) were reported using the inverse normal cumulative distribution. Such function projects a p-value into the space of a normally distributed variable. This makes easy the interpretation and visualization of the results because it visually enlarges the differences across significant regions. For a p-value of 0.05 corresponds a Z value of 1.64, while for a p-value of 0.001 corresponds a Z value of 3.1.

Results

The results of the source analysis are presented in Figs. 3, 4, 5 respectively for each face category: unfamiliar, newly learned and acquaintances. For unfamiliar faces (Fig. 3) the source analysis revealed generators in fMRI-defined ROIs for the early and middle time window responses, but not for the late time interval. The fMRI-defined ROIs that contributed to the early response (150–210 ms) were the Fus bilaterally, the left pSTS, left InfOcc and the PC bilaterally (Fig. 3). Other brain areas (i.e. the visual cortex) also contributed to the solution. The localization of these sources is described in Table 1. The solution for the middle time window (300–380 ms) seems to be similar, including the Fus,

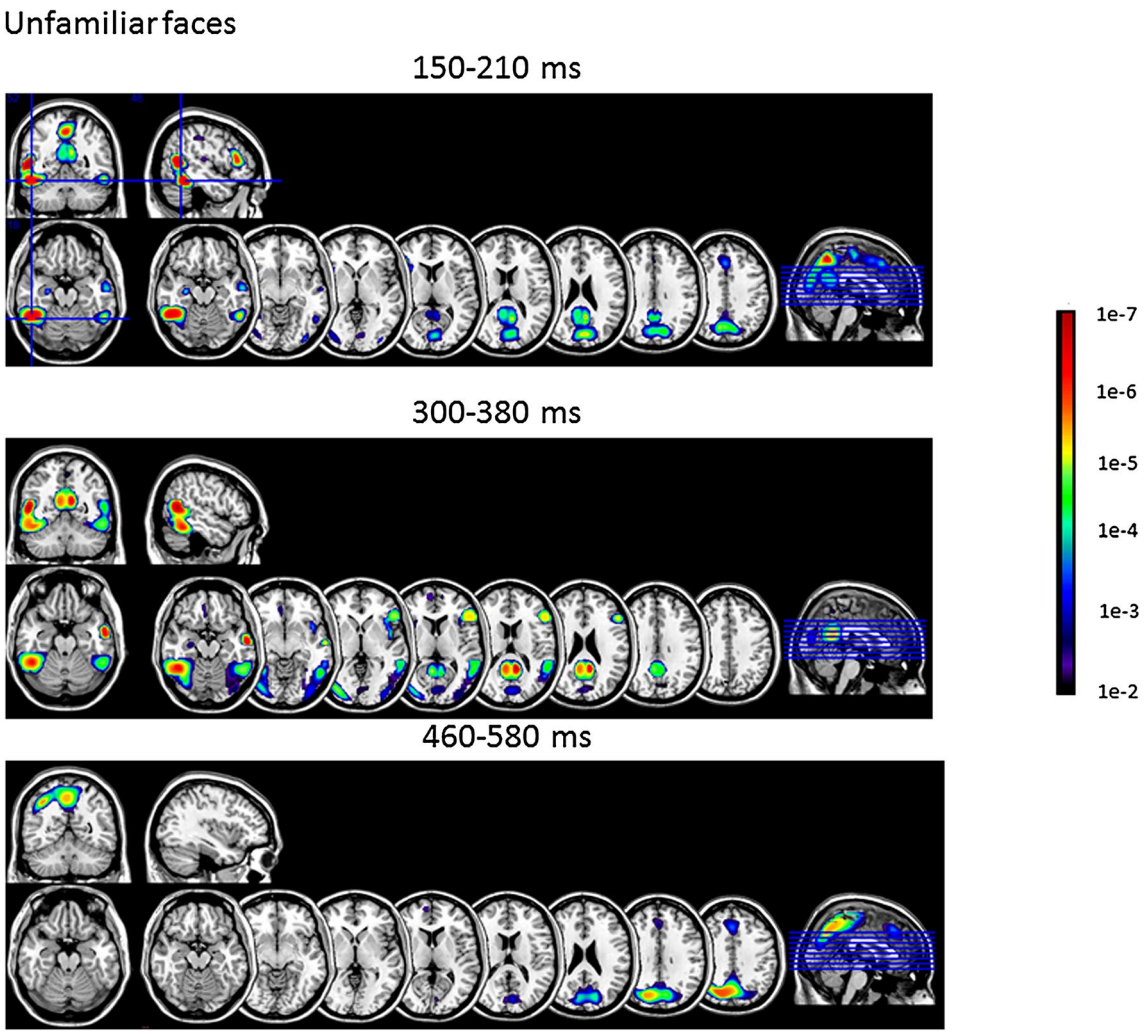

Fig. 3 Statistical maps of the cortical current density distribution of the ERPs to unfamiliar faces. This and subsequent figures present the *Z score* statistical maps for the three time windows analyzed. The Z scores were obtained by transforming the permutation derived *p values* using the inverse of the Gaussian cumulative density. Only those voxels where the Z value reached significance (Z = 3.1, p value = 0.001) are displayed. This and subsequent maps were plotted with MRIcron (http://www.sph.sc.edu/comd/rorden/mricron)

InfOcc, the PC bilaterally and right pSTS (Fig. 3), and also includes other brain areas (see Table 1). The most consistent sources across subjects at the late response (460–580 ms) were located in the Supp Motor Area and Precuneus, without participation of any fMRI-defined areas.

For newly learned faces sources of the early response were estimated in Fus bilaterally, right ATempM and in the left PC (Fig. 4), with small contributions of other brain structures out of the fMRI pre-defined space (Table 2). For the middle time window, several generators were located in the fMRI pre-defined regions, including the right ATempM, the bilateral FrInfT, and bilateral AC. In this case other sources were localized in brain areas out of the fMRI-defined space, such as the bilateral Supplementary Motor Area (see Table 2). For the late response, the most significant sources were located out of the fMRI-defined ROIs, with the main sources localized in Postcentral Area and Middle Cingulate gyrus (see Table 2).

The sources of the three different ERP components elicited by faces of acquaintances are shown in Fig. 5. For this face category, sources of the early response were found in fMRI-defined ROIs: the bilateral Fus, the right OccInf, bilateral mOF, bilateral AC, bilateral PC, left Hip and right ATempM (Table 3). The sources of the middle time window response (300–380 ms) were very similar and located bilaterally in Fus, mOF, AC, FrInfT, PC, ATempM, Ins and Hip, and also small clusters in right pSTS and right InfOcc. Other areas from central and visual cortices also contributed to this component (see Table 3). The solution obtained for the late response elicited by face of acquaintances found

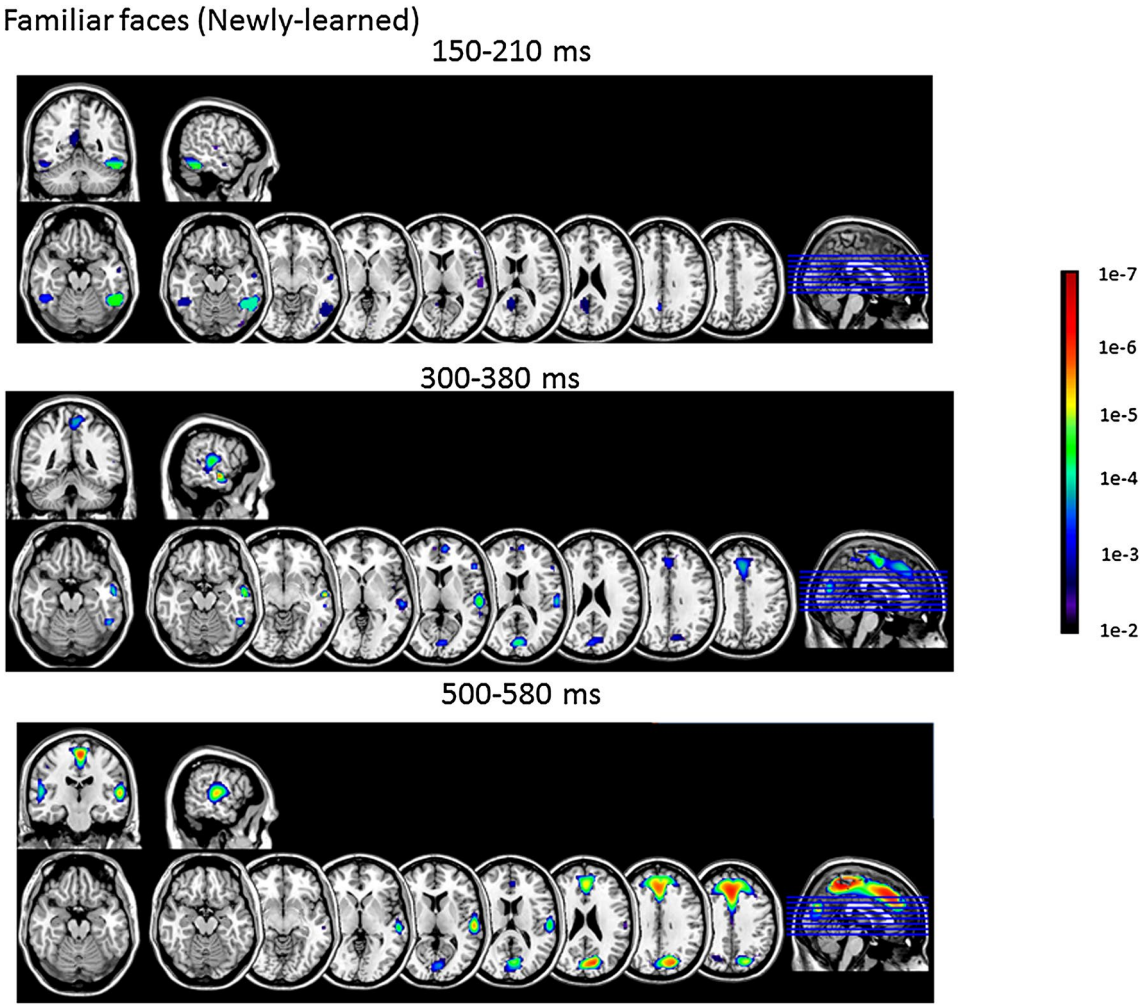

Fig. 4 Statistical maps of the cortical current density distribution of the ERPs to newly-learned faces

generators out of the fMRI-defined ROIs explored here, but their locations differed to those described previously for newly learned and unfamiliar faces. In this case, the most significant sources were located in the central part of the Temporal Middle gyrus bilaterally (see Table 3).

In order to quantify the magnitude of the source activations in the face system ROIs, a cluster-mass index was measured within each area. The results from this analysis are assembled in Fig. 6, where the response of each ROI at each time window is represented with a bar graph for each face category. For unfamiliar faces, in the early and middle time windows (150–210 ms and 300–380 ms) large cluster mass values were found in face-selective areas (Fus, InfOcc, pSTS), as well as in the left PC. The highest cluster mass values were found in the middle time window, in which also the ATempM and FrInfT showed large values. No important activation of any of the fMRI-defined ROIs was observed in the late time window (460–580 ms). For newly-learned faces, in the early time window (150–210 ms) highest cluster mass values were found in bilateral Fus, right ATempM and left PC, and a discrete value was observed in the right InfOcc. In the middle time window (300–380 ms), higher activation appeared in the ATempM area, and also small cluster mass values could be observed in right Fus, bilateral AC, and bilateral FrInfT ROIs. In the late time window (500–580 ms), no activation in the fMRI-defined ROIs was observed (except for the left FrInfT area). For faces of acquaintances, ROIs of both core and extended face systems showed higher cluster mass values in the two earlier time windows. In the first one (150–210), highest cluster mass values were associated with right Fus, bilateral mOF, right PC and ATempR, and smaller values were found in left Fus, right InfOcc, bilateral AC, left FrInfT and bilateral Hip. Increased cluster mass values were observed in the middle time window (300–380 ms), where bilateral mOF and bilateral AC showed the highest values, but important activations were also present in ATempM, bilateral FrInfT, Ins, Hip, left PC and in right Fus and right pSTS. In the late time window

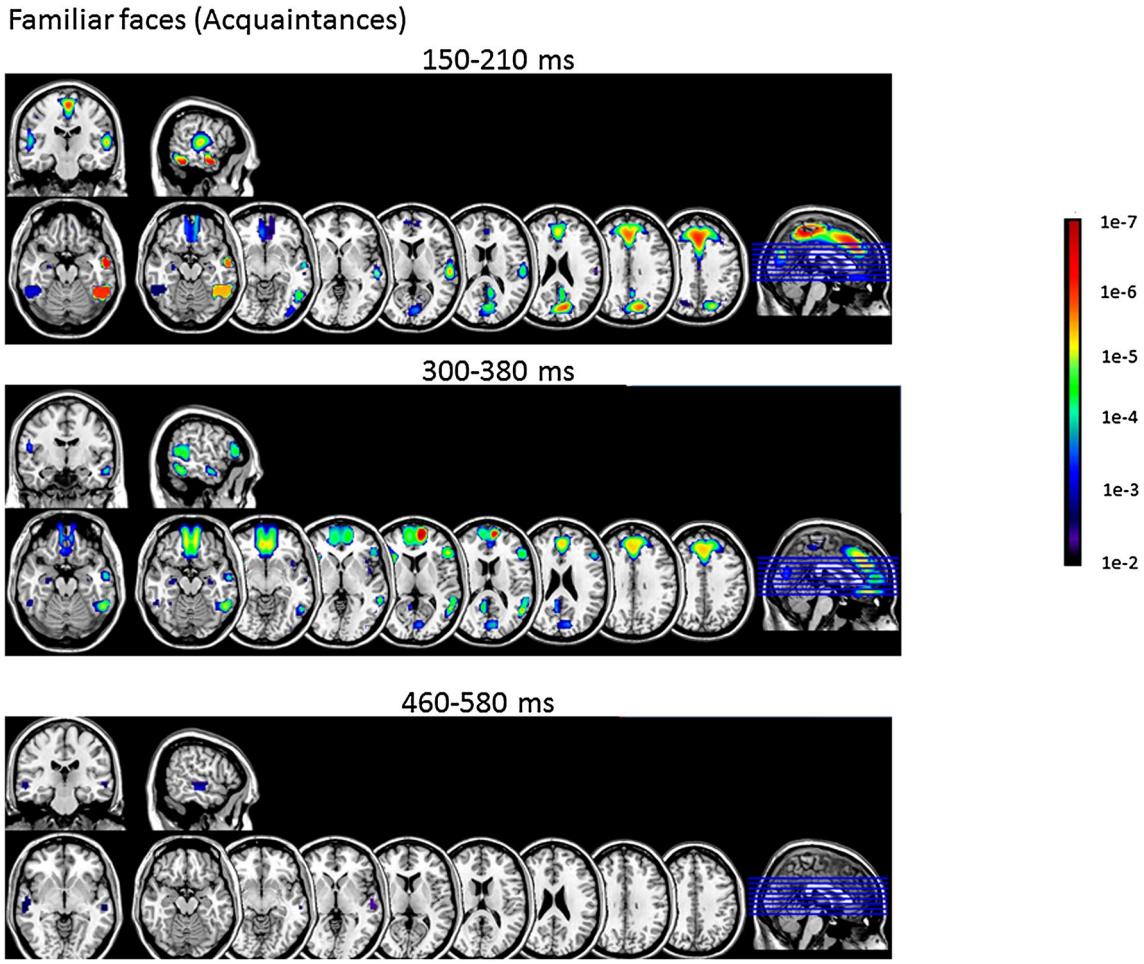

Fig. 5 Statistical maps of the cortical current density distribution of the ERPs to faces of acquaintances

(460–570) no significant cluster mass values showed up in any of the fMRI-defined ROIs, which is similar to the result obtained for other face categories.

Discussion

To infer the temporal dynamics of familiar face processing, we used a BMA/ fMRI guided inverse solution method to assess the contribution of fMRI defined areas (Bobes et al. 2013) to the generation of ERPs elicited by faces with varying levels of familiarity in three time windows (150–210 ms, 300–380 ms, 460–580 ms). This fMRI-defined ROIs coincide with those described in the neural model for familiar face recognition (Gobbini and Haxby 2007) and belong either to the core or to the extended face system.

The present study complement our two previous studies in which we obtained information about the processing of different types of information associated to familiar faces, by recording either ERPs or fMRI related to unfamiliar, visually familiar, and personally-familiar faces. In the previous ERP study (Bobes et al. 2007) we found that all three types of faces evoked an early ERP response, whose amplitude was not modulated by familiarity (probably the N170). In addition, personally-familiar faces elicited two components: a frontal positive response around 300 ms, and a later centro-parietal positive response around 500 ms, whereas visually familiar faces only elicited the later response. The topography of these responses was different, arguing for differences in active neural source configurations. These results suggested that information related with different face memories is accessed at different times in different neural structures/ networks. However, ERP topography does not allow to make inferences regarding the precise anatomical location of the nodes of these networks.

On the other hand, fMRI responses to unfamiliar, visually familiar, and personally-familiar faces (Bobes et al. 2013) demonstrated that most areas of the extended face processing system (medial orbito-frontal, anterior and posterior cingulate) exhibited higher amplitude and prolonged

Table 1 Local maxima of the clusters of generators estimated for unfamiliar faces

(a) 150–210 ms							
fMRI-ROI clusters	Z max	n voxels (ROI %)	Maximum location	X	Y	Z	Other structures included in the cluster
FrInfT L	3.78	3176 (18%)	Frontal Inf Tri L	-46	28	13	-
PC L PC R	4.25	5335 (15%)	Precuneus L	0	-58	24	Cingulum Mid R Cingulum Post L, R Calcarine L, R Cuneus L, R Precuneus R
Fus L	4.44	9598 (15%)	Temporal Inf L	-51	-49	-11	Fusiform L Temporal Mid L
Fus R	3.69	948 (2%)	Temporal Inf R	54	-50	-17	-
(a) 150–210 ms							
Other clusters	Z max	n voxels	Maximum location	X	Y	Z	Other structures included in the cluster
	4.28	6998	Precuneus L	0	-60	49	Cingulum Mid L Cuneus L Precuneus R
	3.93	2072	Cuneus L	-3	-79	20	Calcarine L, R Cuneus R Occipital Sup R Precuneus R
(b) 300–380 ms							
fMRI-ROI clusters	Z max	n voxels (ROI %)	Maximum location	X	Y	Z	Other structures included in the cluster
ATempM R	4.75	4466 (60%)	Temporal Mid R	57	-6	-18	Temporal Sup R Temporal Pole Mid R Temporal Inf R
PC L PC R	5.39	20,636 (78%)	Precuneus R	0	-53	21	Cingulum Mid L, R Cingulum Post L, R Calcarine L, R Cuneus L, R Lingual L, R Precuneus L
Fus L OccInf L	5.16	37,355 (0.6%)	Temporal Inf L	47	-58	-7	Lingual L Occipital Mid L Occipital Inf L Fusiform L Temporal Mid L
Fus R OccInf R pSTS R	4.48	206 (36%)	Temporal Inf R	54	-51	-4	Occipital Inf R Fusiform R Temporal Sup R Temporal Mid R
(b) 300–380 ms							
Other clusters	Z max	nvoxels	Maximum location	X	Y	Z	Other structures included in the cluster
	4.63	8120	Frontal Inf Tri R	51	28	11	Frontal Mid R Frontal Inf Oper R Insula R
(c) 460–580 ms							
fMRI-ROI clusters	Z max	n voxels (ROI %)	Maximum location	X	Y	Z	Other structures included in the cluster
FrInfT L	3.40	181 (1%)	Frontal Inf Tri L	−45	27	12	-
(c) 460–580 ms							
Other clusters	Z max	nvoxels	Maximum location	X	Y	Z	Other structures included in the cluster
	3.31	595	Temporal Sup R	-58	-21	-3	-

Table 1 (continued)

(c) 460–580 ms							
Other clusters	Z max	nvoxels	Maximum location	X	Y	Z	Other structures included in the cluster
	3.52	2076	Temporal Mid L	57	-17	-5	-

In this and subsequent tables we presented clusters corresponding to functional ROIs (fMRI-ROI) and other clusters not included in fMRI-defined areas. Information associated to each cluster are: the maximum Z reached; the number of voxels activate in each cluster (for fMRI-ROI also the percent that number represents from the total size of the ROI); the anatomical label of the maximum in each cluster; MNI coordinates of the maximum; and when clusters included other anatomical structures, they will be also specified in an additional column. Anatomical labels were obtained from the AAL atlas distributed with MARSBAR toolbox (http://marsbar.sourceforge.net/)

Size is the number of voxels belonging to the cluster. For face functional ROIs the percent of the total volume of the ROI is showed

Anatomical labels were obtained from the AAL atlas distributed with MARSBAR toolbox (http://marsbar.sourceforge.net/)

Xmm, Ymm, Zmm are coordinates in MNI space

Blood-Oxygen-Level-Dependent (BOLD) responses to personally-familiar faces but not to visually familiar faces. By contrast, the core face processing areas (OFA and FFA) responded to personally-familiar and visually familiar faces (and also unfamiliar faces) with equivalent amplitude and duration (Bobes et al. 2013). However, the low temporal resolution of the fMRI data does not allow examining changes in the latency of the BOLD response across different areas. Therefore, it was not possible to examine the temporal dynamics of the face circuitry using fMRI.

The present ERPs source analysis contribute to disentangle the temporal sequence of activation of these different areas. Here we found that fMRI defined ROIs contributed to the generation of ERPs in the early (150–210 ms) and middle time windows (300–380 ms), whereas ERPs in the late time window (460–580 ms) were generated in other brain areas. Moreover, for unfamiliar faces only face-selective ROIs (the core face system) contributed to the generation of ERPs in the early and middle time windows, while for familiar faces both the core and extended face system ROIs contributed to the generation of the early and middle ERP responses. However, in the early time window ROIs of the extended system contributed differently to ERP responses to personally familiar compared to only visually familiar faces, with a reduced set of generators in ATempM and PC for newly-learned faces, and a wider set of regions including also the mOF and AC for personally familiar faces. The activation of these areas became even broader in the middle time window for this particular face category.

By modeling plausible ERP generators in fMRI-defined ROIs, we inferred the temporal activation profile of these regions making the best possible use of the data's degrees of freedom. Importantly, even when higher a priori probability was assigned to fMRI-defined ROIs (as the most likely locations), other possible sources could still be localized, since other brain areas were not excluded from the model. Note that the late response (460–580 ms) was not generated in the fMRI defined ROIs (which could be consider the face system), which indicated that this late component is not related to familiar face processing, and must be indexing other type of processing i.e. the organization of behavioral response. Since these late component seem to be unrelated to familiar face processing, these results will not be considered further in this discussion.

ERPs in the early and middle time windows were generated in ROIs of the core and the extended face processing network, but the relative contribution and onset latency of each fMRI defined ROI differed between unfamiliar, newly-learned and acquaintances faces. For unfamiliar faces, generators were found in Fus, InfOcc and pSTS (areas of the face core system), and the participation of the extended face system was restricted to the PC. The core face system have been proposed to participate in the earlier processing of face, and it is related with coding visual appearance and the invariant features of faces (Gobbini and Haxby 2007; Haxby et al. 2000). The early onset response we found in these areas is congruent with this proposal. For newly-learned faces and for faces of acquaintances, the contribution of fMRI defined areas of the core system in the early time window (150–210 ms) was restricted to the Fus, whereas several ROIs of the extended face system also contributed to this early component. Particularly, for personally familiar faces, there were generators of the early ERPs components in all fMRI defined ROIs of the extended system, while only the ATempM and PC contributed for newly-learned faces. These findings are in line with the fact that faces of acquaintances convey more information (semantic, emotional and episodic) than faces learned in the laboratory. It is interesting to note that both mOF and ATempM contributed to the generation of the early response (150–210 ms) to faces of acquaintances, thereby suggesting that the timing of processing of personally significant information (such as emotional reward and other memories) is in the same time interval than the structural information processing of unfamiliar faces (between 150 and 210 ms). It is possible that in this time interval the

Table 2 Local maxima of the clusters of generators estimated for newly-learned faces

(a) 150–210 ms							
fMRI-ROI clusters	Z max	n voxels (ROI %)	Maximum location	X	Y	Z	Other structures included in the cluster
ATempM R	3.56	652 (9%)	Temporal Mid R	59	-9	-13	Temporal Sup R
PC L	3.73	3791 (10%)	Precuneus L	-7	-53	21	Cingulum Post L Calcarine L Cuneus L
Fus L	3.66	2369 (4%)	Temporal Inf L	-49	-47	-20	Fusiform L Temporal Inf L
Fus R	4.28	6476 (11%)	Temporal Inf R	52	-52	-16	Occipital Inf R Fusiform R Temporal Mid R
OccInf R	3.11	53 (0.1%)	Occipital Inf R	38	-82	-16	Occipital Inf R
(a) 150–210 ms							
Other clusters	Z max	n voxels	Maximum location	X	Y	Z	Other structures included in the cluster
	3.94	6079	Temporal Mid L	-56	-19	1	Frontal Inf Oper L Rolandic Oper L Heschl L Temporal Sup L
	3.32	229	Calcarine R	3	-80	4	Calcarine L, R Lingual L,R
	3.33	318	Temporal Sup R	58	-19	7	Rolandic Oper R Heschl R
(b) 300–380 ms							
fMRI-ROI clusters	Z max	n voxels (ROI %)	Maximum location	X	Y	Z	Other structures included in the cluster
ATempM R	4.71	2028 (27%)	Temporal Mid R	59	-9	-15	Temporal Sup R Temporal Pole Mid R
FrInfT L	4.02	1441 (8%)	Frontal Inf Tri L	-46	28	11	-
FrInfT R	3.87	712 (5%)	Frontal Inf Tri R	51	29	11	-
AC R	3.88	1314 (4%)	Frontal Sup Medial R	4	56	11	Frontal Sup Medial L, R Cingulum Ant L, R
Fus R	3.98	1002 (2%)	Temporal Inf R	52	-51	-16	Fusiform R
(b) 300–380 ms							
Other clusters	Z max	nvoxels	Maximum location	X	Y	Z	Other structures included in the cluster
	4.26	5040	Temporal Sup R	58	-23	7	Rolandic Oper R Postcentral R SupraMarginal R Heschl R Temporal Mid R
	3.14	33	Temporal Sup L	-56	-15	-0	Temporal Mid L
	4.08	5593	Cuneus L	4	-80	20	Calcarine L, R Cuneus R Lingual L Occipital Sup R Precuneus R

Table 2 (continued)

(b) 300–380 ms							
Other clusters	Z max	nvoxels	Maximum location	X	Y	Z	Other structures included in the cluster
	4.33	27,019	Supp Motor Area R	2	-2	54	Precentral R Frontal Sup L, R Supp Motor Area L Frontal Sup Medial L, R Cingulum Ant L, R Cingulum Mid L, R Postcentral R Parietal Sup R Precuneus L, R Paracentral L, R
(c) 500–580 ms							
fMRI-ROI clusters	Z max	n voxels (ROI %)	Maximum location	X	Y	Z	Other structures included in the cluster
FrInfT L	3.50	945 (5%)	Frontal Inf Tri L	-46	25	16	
(c) 500–580 ms							
Other clusters	Z max	nvoxels	Maximum location	X	Y	Z	Other structures included in the cluster
	4.08	10,117	Postcentral L	-54	-18	14	Precentral L Frontal Mid L Frontal Inf Oper L Rolandic Oper L Postcentral L SupraMarginal L Heschl L Temporal Sup L Temporal Mid L
	4.58	8120	Temporal Sup R	58	-21	9	Rolandic Oper R Postcentral R SupraMarginal R Heschl R Temporal Sup R Temporal Mid R
	5.06	126,255	Cingulum Mid R	2	-16	47	Precentral L, R Frontal Sup L, R Frontal Mid L, R Supp Motor Area L, R Frontal Sup Medial L,R Cingulum Ant L, R Cingulum Mid L, R Calcarine L, R Cuneus L, R Lingual L Occipital Sup L, R Occipital Mid L, R Postcentral L, R arietal Sup L, R Parietal Inf L, R Angular L, R Precuneus L, R Paracentral Lobule L,R

The corresponding funtional ROI (fMRI-ROI) of each cluster, the anatomical label of the maximum and other anatomical structures included in each cluster are specified

Table 3 Local maxima of the clusters of generators estimated for faces of acquaintances

(a) 150–210 ms							
fMRI-ROI clusters	Z max	n voxels (ROI %)	Maximum location	X	Y	Z	Other structures included in the cluster
ATempM R	5.16	3737 (49%)	Temporal Mid R	57	-7	-18	Temporal Sup R Temporal Pole Mid R Temporal Inf R
Hip L	3.44	200 (2%)	Hippocampus L	-27	-13	-18	-
FrInfT L	3.62	567 (3%)	Frontal Inf Tri L	-45	32	7	-
mOF R mOF L AC L AC R	3.98	8064 (34%)	Frontal Med Orb R	1	46	-12	Frontal Sup Orb L Olfactory L, R Frontal Med Orb L Rectus L, R Cingulum Ant L, R
AC L AC R	3.40	438 (2%)	Frontal Sup Medial L	− 4	57	8	Cingulum Ant L, R Frontal Sup Medial L, R
PC R	4.33	4320 (10%)	Precuneus R	7	-56	22	Cingulum Mid R Calcarine L R Cuneus R Lingual R Precuneus L ,R
Fus R OccInf R	5.04	9600 (17%)	Temporal Inf R	50	-52	-16	Occipital Inf R Fusiform R Temporal Mid R
Fus L	3.69	2930 (5%)	Temporal Inf L	-51	-48	-20	Fusiform L
InfOccR	3.83	1401 (3%)	Occipital Inf R	38	-83	-8	Occipital Mid R
(a) 150–210 ms							
Other clusters	Z max	nvoxels	Maximum location	X	Y	Z	Other structures included in the cluster
	3.17	49	Temporal Mid L	-57	-20	-1	Temporal Mid L
	3.13	69	Temporal Sup R	57	-22	0	Temporal Sup R
(b) 300–380 ms							
fMRI-ROI clusters	Z max	n voxels (ROI %)	Maximum location	X	Y	Z	Other structures included in the cluster
ATempM R	4.24	2173 (29%)	Temporal Mid R	57	-7	-18	Temporal Sup R Temporal Pole Mid R
Hip L	3.54	470 (4%)	Hippocampus L	-27	-14	-17	-
Hip R	3.30	231 (1%)	Hippocampus R	30	-15	-16	-
Ins R	3.98	834 (4%)	Insula R	41	12	-3	-
FrInfT L	4.48	11,409 (64%)	Frontal Inf Tri L	-42	23	9	Frontal Inf Oper L Insula L
FrInfT R	4.64	6412 (38%)	Frontal Inf Tri R	51	29	12	Frontal Mid R Frontal Inf Oper R
AC L AC R mOF L mOF R	5.38	77,859 (100%)	Cingulum Ant L	-1	44	17	Frontal Sup L, R Frontal Sup Orb L, R Frontal Mid L, R Frontal Mid Orb L, R Supp Motor Area L, R Olfactory L, R Frontal Sup Medial L, R Frontal Med Orb L, R Rectus L, R Cingulum Ant L, R Cingulum Mid L, R Caudate L

Table 3 (continued)

(b) 300–380 ms							
fMRI-ROI clusters	Z max	n voxels (ROI %)	Maximum location	X	Y	Z	Other structures included in the cluster
PC L	4.22	3410 (10%)	Precuneus L	-7	-52	18	Cingulum Post L Calcarine L Cuneus L
pSTS R	4.76	11,782 (17%)	Temporal Mid R	54	-52	-1	Occipital Inf R Fusiform R Temporal Sup R Temporal Inf R
Fus L	3.47	674 (1%)	Temporal Inf L	-52	-46	-20	-
Fus R	3.13	29 (0.05%)	Fusiform R	32	-48	-16	
InfOccR	3.41	67 (0.1%)	Occipital Inf R	39	-83	-3	Occipital Mid R
(b) 300–380 ms							
Other clusters	Z max	n voxels	Maximum location	X	Y	Z	Other structures included in the cluster
	3.74	2958	Paracentral Lobule R	1	-38	61	Supp Motor Area R Cingulum Mid L, R Precuneus L, R Paracentral Lobule L
	3.99	5369	Cuneus R	5	-81	17	Calcarine L, R Cuneus L Lingual L
	4.07	6089	Postcentral L	-54	-19	14	Precentral L Rolandic Oper L SupraMarginal L Heschl L Temporal Sup L Temporal Mid L
(c) 460–570 ms							
fMRI-ROI clusters	Z max	n voxels (ROI %)	Maximum location	X	Y	Z	Other structures included in the cluster
FrInfT L	3.40	181 (1%)	Frontal Inf Tri L	-45	27	12	
(c) 460–570 ms							
Other clusters	Z max	nvoxels	Maximum location	X	Y	Z	Other structures included in the cluster
	3.52	2076	Temporal Mid L	− 57	-17	-5	Temporal Sup L
	3.31	595	Temporal Sup R	58	-21	-3	Temporal Mid R

In this and subsequent tables the corresponding funtional ROI (fMRI-ROI) of each cluster, the anatomical label of the maximum and other anatomical structures included in each cluster are specified

two types of processing run in parallel. Another interesting finding is that the contribution of the fMRI-defined ROIs to the ERPs in the middle time window was more extended and reliable than to the ERPs in the early time window, as indicated by the largest values of the cluster mass for unfamiliar faces in the core system ROIs and for faces of acquaintances in the extended system ROIs, suggesting a sustained processing in some areas with the posterior recruitment of additional areas.

Our results suggest a dynamic network with rapid activation growing over time by recruiting further units and nodes according to the memories conveyed by the different types of faces. As predicted by the Gobbini and Haxby model (Gobbini and Haxby 2007), responses to unfamiliar faces in the core face system (FFA, OFA, STS) occur early and are sustained in time. The core system (through right FFA) is also engaged in familiar face processing early in time together with areas of the extended face system triggered by familiar

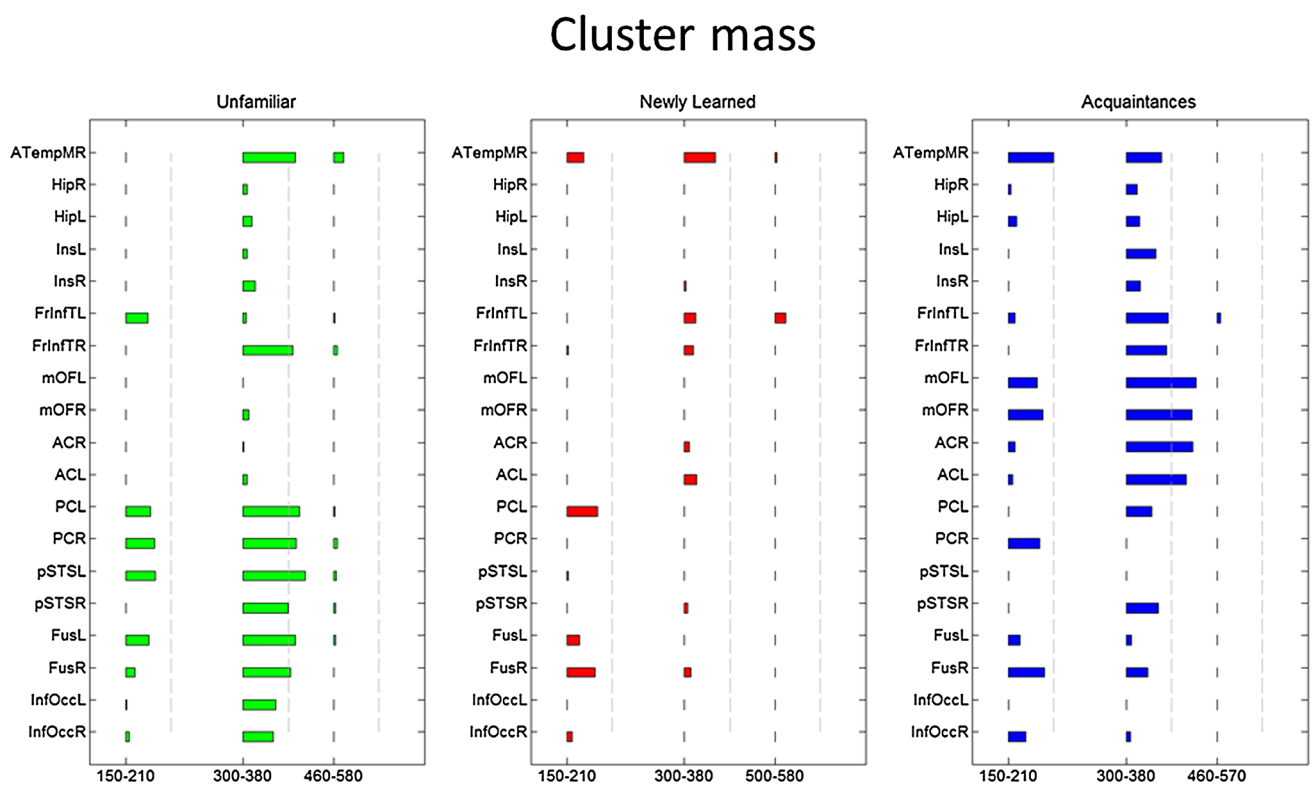

Fig. 6 Cluster mass values representing the ROI contribution to the generation of the ERP components in each time window and face condition. The length of each bar corresponds to the cluster mass intensity at each ROI after thresholding the Kolmogorov–Smirnov (KS) statistic map with the threshold obtained with the permutation procedure. The cluster mass intensity integrates the extent and the amplitude of the response within the ROIs

face processing: PC and ATempM, as well as the mOF for personally significant faces, probably involved in emotional reaction to familiar faces. The remaining structures of the extended face system (e.g., AC, Hip, Ins, FrInfT), possibly involved in processing semantic and episodic information, as well as personal traits and intentions, may be recruited later in time.

From a methodological point of view, different aspects deserve comments. We will first consider the advantage of BMA over traditional source analysis methods and the interest of this approach for fMRI-constrained analysis, and second, we will discuss the statistical method used for the second level analysis. First, the advantage of the BMA method is that a large number of inverse solution maps are weighted by their posterior probability, that is, how well each inverse solution map explains the voltage distribution over the scalp. In this framework, it is possible to address the model uncertainty problem that arises when different model-based solutions account for the same data. Using BMA, it is possible to find a unique inverse solution that is independent (unconditional) of the chosen model (Trujillo-Barreto et al. 2004). Furthermore, BMA general formulation allows defining each model by constraining the solution to a particular anatomical structure or a combination of structures. The prior probability of each model provides information regarding the relative plausibility of the competing models thereby addressing two main problems of linear inverse solutions: (a) the presence of ghost sources in the estimated solution and (b) the tendency to underestimate deep generators in favor of cortical ones (Trujillo-Barreto et al. 2004). Results demonstrate that this strategy seems to cope with both problems. Additionally, it is also possible to consider different prior probabilities for each model based on the fMRI activation maps while maintaining the good properties of BMA (Melie-García et al. 2004). In the present work, we defined prior probabilities assigning the highest values to the face areas defined in a previous fMRI work (Bobes et al. 2013) and lower probabilities to other brain areas, in order to guarantee the inclusion of additional sources, if present. With this approach, the properties of BMA are maintained, since prior odds were set to one in the fMRI-defined ROIs, and since different models resulting from the combination of the fMRI-defined ROIs have the same prior probability. Consequently, while the relative plausibility of the different fMRI-ROIs combinations will be the same, the model favors the brain regions receiving higher support from the data and penalizes those that are less likely to contribute to the generation of the ERP components and deeper ROIs are

not disfavored. The brain areas not included in the fMRI data based ROIs are considered as less likely generators (prior odds were set to 0.5), but the support they receive from the data is taken into account.

Regarding second level analyses, BMA creates a statistical challenge for the estimation of group effects, because the scale of BMA coefficient maps is largely variable across participants. As a consequence, the parametric tests for the group mean are useless. Thus, to assess the statistical significance of group effects, we used non-parametric methods based on the spatial consistency of BMA maps. Rank tests have recently been used by Rosenblatt and co-workers (Rosenblatt et al. 2014) for fMRI data second level analysis. These authors demonstrated that the rank test increases statistical power compared with conventional parametric methods, when the data follow a mixture model of active and non-active populations of unknown distribution functions (Xu et al. 2009). Importantly, in the present study, we also estimated statistical significance at each voxel with permutation tests to avoid the problems of sample size requirements and the assumption of dependence of the distribution of BMA maps. To the best of our knowledge, no other methods allow overcoming the differences in variation scale of BMA maps.

The present results obtained with the method described above are consistent with other studies using more traditional inverse solution approaches. Previous studies performing source analysis using distributed solutions models without restricting the space of solutions found that the Fus (Corrigan et al. 2009; Caldara et al. 2003; Herrmann et al. 2005; Henson et al. 2007), STS (Itier and Taylor 2004; Corrigan et al. 2009; Eryilmaz et al. 2007), OFA (Henson et al. 2007, 2009; Caldara et al. 2003; Corrigan et al. 2009; Herrmann et al. 2005) and also the PC (Corrigan et al. 2009) contributed to the N170 to unfamiliar faces. These results are in line with the sources found here in the early time window that included the N170 component. Results obtained using dipolar models are also congruent with the present results. Generators of the N170 to unfamiliar faces were located in the fusiform and inferior occipital gyrus (Shibata et al. 2002; Rossion et al. 2003; Deffke et al. 2007; Jemel et al. 2009; Caldara et al. 2003). Dipole analysis of the N250 component related to familiarity processing (Schweinberger et al. 2002) revealed that the Fus was the main generator. Other studies also described the implication of the inferior frontal regions in the ERPs responses to familiar faces in different tasks (Mnatsakanian and Tarkka 2004; Genetti et al. 2009; Jemel et al. 1999; Tarkka and Mnatsakanian 2003; Gao et al. 2013).

Due to the uncertainty of inverse solution models, a gold standard is to use data obtained from intracranial recordings. Importantly, the present results are in line with those reported by Barbeau and collaborators (Barbeau et al. 2008) in an exhaustive study of the electro-cortical responses to faces. These authors found responses to familiar and unfamiliar faces with different latencies in several areas of the face system. The earliest response to both familiar and unfamiliar faces (around 110 ms) was found in the Fus, InfOcc regions and in the inferior frontal gyrus. A familiarity effect was found between 250 and 360 ms in areas of the temporal pole and hippocampus. Other studies using intracranial recordings also found early activations for faces in the Fus and late activations in a widespread network (Puce et al. 1996, 1999; Halgren et al. 1994; Allison et al. 1994, 1999; Dietl et al. 2005). Importantly, however, intracranial recording studies have not explored other structures of the extended face system (e.g., AC, FrInfT and PC), which in the present study were found to contributes also to face elicited ERPs.

Additional evidence suggests multiple contribution of different areas of the core face system to the N170 component, including adaptation studies in normal participants (Eimer et al. 2010) and studies in patients with acquired prosopagnosia (Dobel et al. 2008; Dalrymple et al. 2011; Oruc et al. 2010; Bobes et al. 2004).

The results obtained here evince the potential of the fMRI-guided BMA solution for exploring temporal dynamics in neural cognitive networks. However, some methodological aspect would be improved. In this study, we defined the ROIs from the group analysis, in order to have a common solution space that facilitated the sources statistical analysis. Also, the ERP component for source estimation (the time window presenting experimental condition effects) were selected from group analysis. It could be convenient in future studies to select the ROI and locate the time presenting effects, individually by each subject. By this way, the spatial and temporal variability of the data due to anatomical variations of functional areas and differences in temporal processing will be minimized, allowing more precise results.

In sum, our results provide additional information regarding the temporal-dynamics of the familiarity processing in the neural system for familiar face recognition. Face processing models have tried to posit the nodes of the face circuitry and the computations carried out in each node. As these models are based on fMRI studies, they fully described the different neural structures that participate in the processing of different types of information derived from faces. However, no temporal information was included. The temporal dynamics described here complements those models. The simplest hypothesis is that response onset latency increases as activation progresses along the ventral visual pathway, integrating the core system with frontal areas belonging to the extended face system. This hypothesis is not entirely supported by the present data. While response onset latency differs between ROIs, fast responses were found not only in areas of the core system but also in areas of the extended

face system. As the earliest analyzed time window was 150–210 ms, it is possible that response onset latency was shorter (inferior to 150 ms). Previous results suggested an early ERP face modulation around 100 ms (P100) and sources analysis using LORETA localized P100 generators in the Fus (Herrmann et al. 2005). Thus, activation in the Fus may occur before the mOF. Nevertheless, results of intracranial studies showed activation of these two structures at the same latency. Moreover, considering LORETA problems for localizing deep sources such as mOF (see Trujillo-Barreto et al. 2004 for a discussion), the possibility of simultaneous activation of Fus and mOF cannot be discarded.

Conclusion

The present study suggested that the processing of different types of faces involves a complex network, including areas of the core and the extended face systems that operates in parallel and acts dynamically. We concluded that fMRI-constrained BMA source analysis provides information about the temporal-dynamics of the neural system for familiar face recognition, which complement the anatomical information considered in the currently accepted model.

Acknowledgements The present study was partly supported by a scientific collaboration program between the Cuban Neuroscience Center and the Autonomous University of Madrid and by the Grant No. 81330032 from the National Nature Science Foundation of China NSFC.

References

Allison T, Ginter H, McCarthy G, Nobre AC, Puce A, Luby M, Spencer DD (1994) Face recognition in human extrastriate cortex. J Neurophysiol 71:821–825

Allison T, Puce A, Spencer DD, McCarthy G (1999) Electrophysiological studies of human face perception. I: potentials generated in occipitotemporal cortex by face and non-face stimuli. Cereb Cortex 9:415–430

Barbeau EJ, Taylor MJ, Regis J, Marquis P, Chauvel P, Liegeois-Chauvel C (2008) Spatio temporal dynamics of face recognition. Cereb Cortex 18:997–1009

Bentin S, Deouell LY (2000) Structural encoding and identification in face processing: erp evidence for separate mechanisms. Cogn Neuropsychol 17:35–55

Bobes MA, Lopera F, Comas LD, Galan L, Carbonell F, Bringas ML, Valdes-Sosa M (2004) Brain potentials reflect residual face processing in a case of prosopagnosia. Cogn Neuropsychol 21:691–718

Bobes MA, Quinonez I, Perez J, Leon I, Valdes-Sosa M (2007) Brain potentials reflect access to visual and emotional memories for faces. Biol Psychol 75:146–153

Bobes MA, Lage CA, Quinones I, Garcia L, Valdes-Sosa M (2013) Timing and tuning for familiarity of cortical responses to faces. PLoS ONE 8:e76100

Brambati SM, Benoit S, Monetta L, Belleville S, Joubert S (2010) The role of the left anterior temporal lobe in the semantic processing of famous faces. Neuroimage 53:674–681

Bullmore ET, Suckling J, Overmeyer S, Rabe-Hesketh S, Taylor E, Brammer MJ (1999) Global, voxel, and cluster tests, by theory and permutation, for a difference between two groups of structural MR images of the brain. IEEE Trans Med Imaging 18:32–42

Caldara R, Thut G, Servoir P, Michel CM, Bovet P, Renault B (2003) Face versus non-face object perception and the 'other-race' effect: a spatio-temporal event-related potential study. Clin Neurophysiol 114:515–528

Corrigan NM, Richards T, Webb SJ, Murias M, Merkle K, Kleinhans NM, Johnson LC, Poliakov A, Aylward E, Dawson G (2009) An investigation of the relationship between fMRI and ERP source localized measurements of brain activity during face processing. Brain Topogr 22:83–96

Dale AM, Sereno MI (1993) Improved localization of cortical activity by combining EEG and MEG with MRI cortical surface reconstruction: a linear approach. J Cogn Neurosci 5:162–176

Dalrymple KA, Oruc I, Duchaine B, Pancaroglu R, Fox CJ, Iaria G, Handy TC, Barton JJ (2011) The anatomic basis of the right face-selective N170 IN acquired prosopagnosia: a combined ERP/fMRI study. Neuropsychologia 49:2553–2563

Deffke I, Sander T, Heidenreich J, Sommer W, Curio G, Trahms L, Lueschow A (2007) MEG/EEG sources of the 170-ms response to faces are co-localized in the fusiform gyrus. Neuroimage 35:1495–1501

Dietl T, Trautner P, Staedtgen M, Vannuchi M, Mecklinger A, Grunwald T, Clusmann H, Elger CE, Kurthen M (2005) Processing of famous faces and medial temporal lobe event-related potentials: a depth electrode study. Neuroimage 25:401–407

Dobel C, Putsche C, Zwitserlood P, Junghofer M (2008) Early left-hemispheric dysfunction of face processing in congenital prosopagnosia: an MEG study. PLoS ONE 3:e2326

Eimer M (2000a) Event-related brain potentials distinguish processing stages involved in face perception and recognition. Clin Neurophysiol 111:694–705

Eimer M (2000b) Effects of face inversion on the structural encoding and recognition of faces. Evidence from event-related brain potentials. Brain Res Cogn Brain Res 10:145–158

Eimer M (2011) The face-sensitivity of the n170 component. Front Hum Neurosci 5:119

Eimer M, Kiss M, Nicholas S (2010) Response profile of the face-sensitive N170 component: a rapid adaptation study. Cereb Cortex 20:2442–2452

Elfgren C, van WD, Passant, Larsson U, Mannfolk EM, Fransson P P (2006) fMRI activity in the medial temporal lobe during famous face processing. Neuroimage 30:609–616

Eryilmaz HH, Duru AD, Parlak B, Ademoglu A, Demiralp T (2007) Neuroimaging of event related brain potentials (ERP) using fMRI and dipole source reconstruction. Conf Proc IEEE Eng Med Biol Soc 2007:3384–3387

Gao Z, Goldstein A, Harpaz Y, Hansel M, Zion-Golumbic E, Bentin S (2013) A magnetoencephalographic study of face processing: M170, gamma-band oscillations and source localization. Hum Brain Mapp 34:1783–1795

Genetti M, Khateb A, Heinzer S, Michel CM, Pegna AJ (2009) Temporal dynamics of awareness for facial identity revealed with ERP. Brain Cogn 69:296–305

Gobbini MI, Haxby JV (2007) Neural systems for recognition of familiar faces. Neuropsychologia 45:32–41

Gobbini MI, Leibenluft E, Santiago N, Haxby JV (2004) Social and emotional attachment in the neural representation of faces. Neuroimage 22:1628–1635

Gorno-Tempini ML, Price CJ (2001) Identification of famous faces and buildings: a functional neuroimaging study of semantically unique items. Brain 124:2087–2097

Halgren E, Baudena P, Heit G, Clarke JM, Marinkovic K, Clarke M (1994) Spatio-temporal stages in face and word processing. I. Depth-recorded potentials in the human occipital, temporal and parietal lobes [corrected]. J Physiol Paris 88:1–50

Haxby JV, Hoffman EA, Gobbini MI (2000) The distributed human neural system for face perception. Trends Cogn Sci 4:223–233

Henson RN, Goshen-Gottstein Y, Ganel T, Otten LJ, Quayle A, Rugg MD (2003) Electrophysiological and haemodynamic correlates of face perception, recognition and priming. Cereb Cortex 13:793–805

Henson RN, Mattout J, Singh KD, Barnes GR, Hillebrand A, Friston K (2007) Population-level inferences for distributed MEG source localization under multiple constraints: application to face-evoked fields. Neuroimage 38:422–438

Henson RN, Mouchlianitis E, Friston KJ (2009) MEG and EEG data fusion: simultaneous localisation of face-evoked responses. Neuroimage 47:581–589

Herrmann MJ, Ehlis AC, Muehlberger A, Fallgatter AJ (2005) Source localization of early stages of face processing. Brain Topogr 18:77–85

Horovitz SG, Rossion B, Skudlarski P, Gore JC (2004) Parametric design and correlational analyses help integrating fMRI and electrophysiological data during face processing. Neuroimage 22:1587–1595

Iidaka T, Matsumoto A, Haneda K, Okada T, Sadato N (2006) Hemodynamic and electrophysiological relationship involved in human face processing: evidence from a combined fMRI-ERP study. Brain Cogn 60:176–186

Itier RJ, Taylor MJ (2004) Source analysis of the N170 to faces and objects. Neuroreport 15:1261–1265

Jemel B, George N, Olivares E, Fiori N, Renault B (1999) Event-related potentials to structural familiar face incongruity processing. Psychophysiology 36:437–452

Jemel B, Coutya J, Langer C, Roy S (2009) From upright to upside-down presentation: a spatio-temporal ERP study of the parametric effect of rotation on face and house processing. BMC Neurosci 10:100

Joyce C, Rossion B (2005) The face-sensitive N170 and VPP components manifest the same brain processes: the effect of reference electrode site. Clin Neurophysiol 116:2613–2631

Kaufmann JM, Schweinberger SR, Burton AM (2009) N250 ERP correlates of the acquisition of face representations across different images. J Cogn Neurosci 21:625–641

Latinus M, Taylor MJ (2006) Face processing stages: impact of difficulty and the separation of effects. Brain Res 1123:179–187

Leveroni CL, Seidenberg M, Mayer AR, Mead LA, Binder JR, Rao SM (2000) Neural systems underlying the recognition of familiar and newly learned faces. J Neurosci 20:878–886

Linkenkaer-Hansen K, Palva JM, Sams M, Hietanen JK, Aronen HJ, Ilmoniemi RJ (1998) Face-selective processing in human extrastriate cortex around 120 ms after stimulus onset revealed by magneto- and electroencephalography. Neurosci Lett 253:147–150

MacKay DJ (1992) Bayesian interpolation. Neural Comput 4(3):415–447

Melie-García L, Trujillo-Barreto NJ, Martínez-Montes E, Koenig T, Valdés-Sosa PA (2004) EEG imaging via BMA with fMRI pre-defined prior model probabilities. In: Human Brain Mapping, Budapest, June

Michel CM, Murray MM, Lantz G, Gonzalez S, Spinelli L, Grave de PR (2004) EEG source imaging. Clin Neurophysiol 115:2195–2222

Mnatsakanian EV, Tarkka IM (2004) Familiar-face recognition and comparison: source analysis of scalp-recorded event-related potentials. Clin Neurophysiol 115:880–886

Oostendorp TF, Delbeke J, Stegeman DF (2000) The conductivity of the human skull: results of in vivo and in vitro measurements. IEEE Trans Biomed Eng 47:1487–1492

Oruc I, Cheung T, Dalrymple K, Fox C, Iaria G, Handy T, Barton J (2010) Residual face-selectivity of the N170 and M170 is related to the status of the occipital and fusiform face areas in acquired prosopagnosia. J Vision 10(7), article 585. https://doi.org/10.1167/10.7.585

Penny WD, Mattout J, Trujillo-Barreto NJ (2006) Chap. 35. Bayesian model selection & averaging. In: Friston KJ et al (eds) Statistical parametric mapping: the analysis of functional brain images. Academic Press, Oxford, pp 454–467

Pizzagalli DA, Lehmann D, Hendrick AM, Regard M, Pascual-Marqui RD, Davidson RJ (2002) Affective judgments of faces modulate early activity (approximately 160 ms) within the fusiform gyri. Neuroimage 16:663–677

Pourtois G, Dan ES, Grandjean D, Sander D, Vuilleumier P (2005a) Enhanced extrastriate visual response to bandpass spatial frequency filtered fearful faces: time course and topographic evoked-potentials mapping. Hum Brain Mapp 26:65–79

Pourtois G, Schwartz S, Seghier ML, Lazeyras F, Vuilleumier P (2005b) View-independent coding of face identity in frontal and temporal cortices is modulated by familiarity: an event-related fMRI study. Neuroimage 24:1214–1224

Puce A, Allison T, Asgari M, Gore JC, McCarthy G (1996) Differential sensitivity of human visual cortex to faces, letterstrings, and textures: a functional magnetic resonance imaging study. J Neurosci 16:5205–5215

Puce A, Allison T, McCarthy G (1999) Electrophysiological studies of human face perception. III: effects of top-down processing on face-specific potentials. Cereb Cortex 9:445–458

Rosenblatt JD, Vink M, Benjamini Y (2014) Revisiting multi-subject random effects in fMRI: advocating prevalence estimation. Neuroimage 84:113–121

Rossion B, Campanella S, Gomez CM, Delinte A, Debatisse D, Liard L, Dubois S, Bruyer R, Crommelinck M, Guerit JM (1999) Task modulation of brain activity related to familiar and unfamiliar face processing: an ERP study. Clin Neurophysiol 110:449–462

Rossion B, Joyce CA, Cottrell GW, Tarr MJ (2003) Early lateralization and orientation tuning for face, word, and object processing in the visual cortex. Neuroimage 20:1609–1624

Rotshtein P, Henson RN, Treves A, Driver J, Dolan RJ (2005) Morphing Marilyn into Maggie dissociates physical and identity face representations in the brain. Nat Neurosci 8:107–113

Schweinberger SR (2011) Neurophysiological correlates of face recognition. In: Calder AJ, Rhodes G, Johnson MH, Haxby JV (eds) The handbook of face perception. Oxford University Press, Oxford

Schweinberger SR, Pickering EC, Jentzsch I, Burton AM, Kaufmann JM (2002) Event-related brain potential evidence for a response of inferior temporal cortex to familiar face repetitions. Brain Res Cogn Brain Res 14:398–409

Shibata T, Nishijo H, Tamura R, Miyamoto K, Eifuku S, Endo S, Ono T (2002) Generators of visual evoked potentials for faces and eyes in the human brain as determined by dipole localization. Brain Topogr 15:51–63

Tarkka IM, Mnatsakanian EV (2003) Functional specialization in the human frontal cortex observed during task anticipation. Neuropsychobiology 48:102–110

Trautmann-Lengsfeld SA, Domínguez-Borràs J, Escera C, Herrmann M, Fehr T (2013). The perception of dynamic and static facial expressions of happiness and disgust investigated by ERPs and fMRI constrained source analysis. PLoS ONE, 8(6):e66997

Trujillo-Barreto NJ, Aubert-Vazquez E, Valdes-Sosa PA (2004) Bayesian model averaging in EEG/MEG imaging. Neuroimage 21:1300–1319

Tzourio-Mazoyer N, Landeau B, Papathanassiou D, Crivello F, Etard O, Delcroix N, Mazoyer B, Joliot M (2002) Automated anatomical labeling of activations in SPM using a macroscopic anatomical parcellation of the MNI MRI single-subject brain. Neuroimage 15:273–289

Xu L, Johnson TD, Nichols TE, Nee DE (2009) Modeling inter-subject variability in FMRI activation location: a Bayesian hierarchical spatial model. Biometrics 65:1041–1051

Zhang Y, van Drongelen W, He B (2006) Estimation of in vivo brain-to-skull conductivity ratio in humans. Appl Phys Lett 89:223903